Characterization and Some Properties of Poly(vinyl chloride)/Sepiolite Nanocomposites

YASEMIN TURHAN, MEHMET DOĞAN, MAHIR ALKAN

Department of Chemistry, Faculty of Science and Literature, Balikesir University, 10145 Balikesir, Turkey

Received: September 27, 2010
Accepted: August 25, 2011

ABSTRACT: Poly(vinyl chloride) (PVC)/sepiolite nanocomposites were prepared using PVC and natural, organo-modified, acid–activated, and calcined sepiolite samples through the solution intercalation method. Thermogravimetric (TG) analysis, UV–vis spectrophotometry, Fourier transform infrared spectroscopy, and scanning electron microscopy were used to determine the thermal stability, optical behavior, interactions, and morphology of samples, respectively. The dispersion of sepiolite in the PVC matrix was examined by X-ray diffraction (XRD) and transmission electron microscopy (TEM). The nanocomposites exhibited higher thermal stability than that of pure PVC. XRD and TEM results showed that sepiolite particles were dispersed in the nanoscaled PVC matrix. The UV–vis spectra showed that the transmission of nanocomposites increased with the sepiolite content and wavelength. The thermal degradation behavior of PVC was investigated by using TG analysis under nonisothermal conditions at different heating rates under a nitrogen atmosphere. The apparent activation energy of samples was determined by using the Kissinger method. The nanocomposite showed higher activation energy than that of pure PVC. The

Correspondence to: Mehmet Doğan; e-mail: mdogan@balikesir.edu.tr.

Contract grant sponsor: Balikesir University Research Fund.
Contract grant number: 2008/20.

results showed that the thermal degradation of PVC was shifted toward higher temperatures with an increase in the amount of sepiolite. © 2011 Wiley Periodicals, Inc. Adv Polym Techn 32: E65–E82, 2013; View this article online at wileyonlinelibrary.com. DOI 10.1002/adv.20271

KEY WORDS: Nanocomposite, Poly(vinyl chloride), sepiolite

Introduction

Poly(vinyl chloride) (PVC) is a common commercial thermoplastic polymer with the second highest output among all synthetic polymeric materials and is extensively used in construction, transportation, and many other industries because of its high stiffness, flame retardancy, and chemical resistance, as well as its low cost.[1,2] Because of inherent disadvantages, such as poor thermal stability and brittleness, PVC is generally compounded with various additives.[2] Various fillers, including elastomers and rubbers such as acrylonitrile-butadiene rubber, chlorinated polyethylene, poly(methyl methacrylate-*co*-methacrylate), and poly(methacrylate-*co*-butylene-styrene), and inorganic nanoparticles, are used to toughen PVC composites. But the introduction of rubbers or elastomers led to a remarkable decrease in the rigidity, strength, and thermal deformation temperature of PVC, combined with an increase in the viscosity and cost.[3]

Many efforts have been made to improve the properties of polymers, which are widely used in automotive, aerospace, construction, and electronic industries because they provide improved mechanical properties (e.g., stiffness, strength) and physical properties over pure polymers.[1,3] Fillers play an important role in modifying the properties of various polymers and lowering the cost of their composites. The effect of fillers on the properties of composites depends on their level of loading, shape and particle size, aggregate size, surface characteristics, and degree of dispersion.[4] The incorporation of inorganic fillers into thermoplastics has been widely practiced in industry to extend them and to improve certain properties.[5] In recent years, organic–inorganic composites, especially nanocomposites, have received great attention because these materials often exhibit unexpected properties.[2] In general, polymer nanocomposites are made by the dispersion of inorganic or organic nanoparticles into either a thermoplastic or a thermoset polymer. Nanoparticles can be three-dimensional spherical and polyhedral nanoparticles (e.g., colloidal silica), two-dimensional nanofibers (e.g., nanotube, whisker), or one-dimensional disk-like nanoparticles (e.g., clay platelet). Such nanoparticles offer enormous advantages over traditional macro- or microparticles (e.g., talc, glass, carbon fibers) because of their higher surface area and aspect ratio, improved adhesion between the nanoparticle and polymer, and lower amount of loading to achieve equivalent properties.[6]

One of the most promising composite systems would be polymer–clay nanocomposites based on organic polymers and inorganic clay minerals consisting of silicate layers.[5] Clay minerals have been widely used and proved to be very effective due to their unique structure and properties. Such minerals include both natural clays (e.g., montmorillonite, hectorite, and saponite) and synthesized clays (e.g., fluorohectorite, laponite, and magadiite).[6] The common ways used to enhance the interfacial interactions of fillers and matrix are (1) modifying the filler surface with coupling agents or polymers, (2) increasing the polarity of the matrix, and (3) introducing a third component with bifunctional properties that can interact with both the filler and matrix.[7–11] The chemistry of silane treatment is described in many publications, and there are three models of grafting. In the first model the first molecule of silane is grafted on the surface of inorganic particles and others are condensed on the one that has been grafted. The second model, which is geometrically impossible, assumes that the silane makes three siloxane bonds. The last and more realistic (the so-called "horizontal") model involves the grafting reaction of the silane and the condensation.[12,13] Moreover, the interfacial interaction between filler particles and polymer matrices and the dispersion of filler particles in polymer matrices play a very important role in improving the toughening efficiency.[3]

The development of nanocomposites based on sepiolite can be the subject of great interest due to

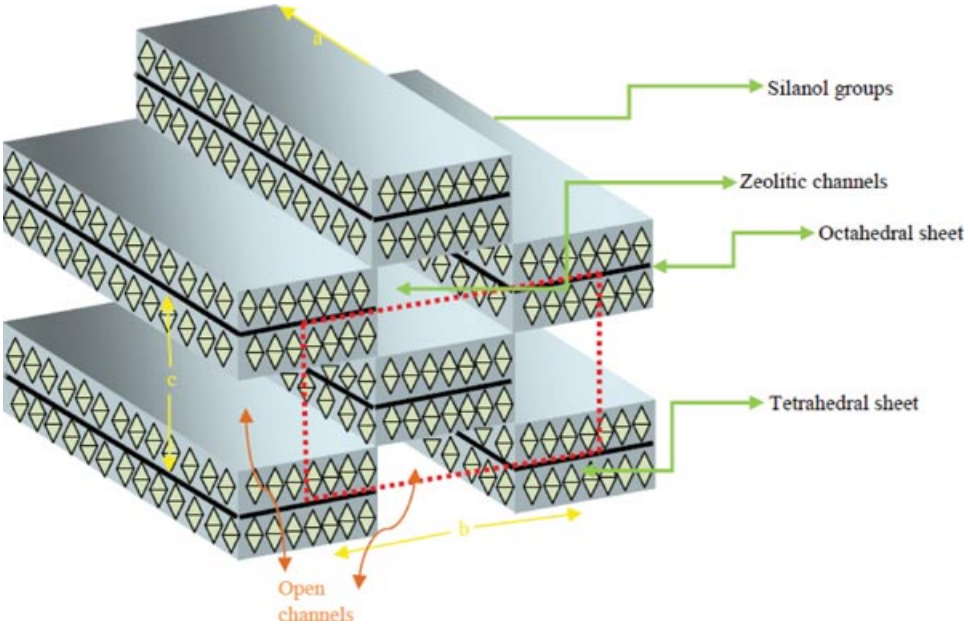

FIGURE 1. Structure of sepiolite.

the special physicochemical characteristics of sepiolite. Sepiolite is a hydrated magnesium phyllosilicate with fibrous morphology resulting from the molecular organization of an ideal unit $Si_{12}O_{30}Mg_8(OH)_4(OH_2)_4 \cdot 8H_2O$. Sepiolite is a natural nanostructural material, and its ideal structure was studied by Bradley early in 1940.[14] The structure of sepiolite, modified from the studies of Bradley, Vivaldi, Ruiz, and Nagy, is shown in Fig. 1.[15,16] According to this formula, sepiolite contains zeolitic and adsorbed water in its structure, four H_2O molecules coordinated with bordering octahedral cations, and hydroxyl groups at the center of the 2:1 ribbons.[17–19] Sepiolite has a high Brunauer–Emmett–Teller (BET) surface area that allows adsorption of water, polar liquids, ions, and even molecules such as drugs or insecticides. Adsorption is due to the presence of active adsorption centers on sepiolite surfaces (oxygen atoms in the tetrahedral sheet, water molecules coordinated with the Mg^{2+} ions at the edge of the structure, and silanol groups caused by the breakup of Si—O—Si bonds).[20,21] In previous studies, Benlikaya et al. investigated the preparation and characterization of sepiolite–poly(ethyl methacrylate) and poly(2-hydroxyethyl methacrylate) nanocomposites[22]; Xie et al., the preparation, structure, and thermomechanical properties of nylon-6 nanocomposites with lamella- and fiber-type sepiolite[23]; Chen et al., properties of sepiolite/polyurethane nanocomposites[3]; Ma et al., preparation of polypropylene/sepiolite nanocomposites using supercritical CO_2-assisted mixing[24]; Aranda et al., titania–sepiolite nanocomposites prepared by using a surfactant templating colloidal route[25]; Santiago et al., the synthesis and swelling behavior of poly(sodium acrylate)/sepiolite superabsorbent composites and nanocomposites[26]; and Darder et al., microfibrous chitosan–sepiolite nanocomposites.[27] In this paper, we aimed to synthesize PVC/sepiolite nanocomposites by (1) modifying the sepiolite particle surfaces with a coupling agent, acid activation, and calcination and (2) the effect of the filler/polymer ratio on properties of PVC/sepiolite nanocomposites. The characterization of PVC/sepiolite nanocomposites was made using X-ray diffraction (XRD) and transmission electron microscopy (TEM), the interactions between sepiolite samples and PVC using Fourier transform infrared spectroscopy (FTIR), the surface areas using a Nova 2200e BET surface area instrument, the thermal properties using simultane differential thermal analysis (DTA)/thermogravimetric (TG) analysis, the optical properties using a UV–vis spectrophotometer, and the morphology using scanning electron microscopy (SEM). Moreover, activation energy values were also determined from differential thermogram values using the Kissinger equation.

Materials and Methods

MATERIALS

The PVC, sepiolite, and dimethyloctadecylchlorosilane (DMODCS) used in this study were purchased from Acros Organics (New Jersey, USA), Merck (Germany), and Fluka (USA), respectively. All other chemicals were of analytical grade and were used without further purification.

METHODS

Modification of Sepiolite with a Silane-Coupling Agent

Sepiolite samples were treated before use in the experiments to obtain a uniformly sized sample. A suspension containing 10 g/L sepiolite was mechanically stirred for 24 h; then after waiting for about 2 min, the supernatant suspension was filtered through filter paper. The solid sample was dried at 105°C for 24 h, ground, and then sieved with a 50-μm sieve. The particles that were less than 50 μm were used for further experiments.[28] Sepiolite (5 g), which was suspended in toluene (100 mL), was refluxed at 80°C and mechanically stirred for 1 h under dry nitrogen. DMODCS (5.0 g) was added dropwise into this suspension. The mixture was refluxed for an additional 24 h, filtered, and washed with toluene, followed by methanol and acetone. The modified sepiolite was dried at 110°C.[19]

Calcination of Sepiolite

Calcined sepiolite samples were prepared at the temperature range of 150–900°C with a Nuve MF-140 furnace.

Acid Activation of Sepiolite

To obtain the acid-activated sepiolite samples, HCl solutions were used. A sepiolite sample of 5 g was treated in 100 mL of 0.5, 1, and 3 M HCl solutions at 25°C for 24 h. Then the suspension was filtered, washed until no chloride anions could be detected, and dried at 110°C for 24 h.[28]

PVC/Organo, Acid-Activated, and Calcined Sepiolite Nanocomposites

For the preparation of PVC/organo, acid-activated, and calcined sepiolite nanocomposites, the solution intercalation method was used. The sepiolite samples of 1, 2.5, and 5 wt% in 50 mL of tetrahydrofuran (THF) solution were added into a reaction vessel. These suspensions were then treated in an ultrasound bath for 20 min. At the same time, 1 g of PVC in 50 mL of THF solution was stirred at room temperature. When the PVC was completely dissolved, the sepiolite sample suspension and PVC solution were mixed together. Then it was stirred at room temperature for 24 h. This suspension was retreated in an ultrasound bath for 20 min. The THF solution was evaporated at 40°C. Finally, PVC/sepiolite nanocomposite films were obtained. All PVC/sepiolite nanocomposites were prepared with the same procedure. In the experiments, the sepiolite amount was 2.5 wt%, except for those in which the effect of the filler amount was investigated.

CHARACTERIZATION OF NANOCOMPOSITES

Characterizations of PVC, sepiolite, and PVC/sepiolite nanocomposites were made according to the methods described below.

XRD Patterns

XRD measurements of samples were performed using an analytical Philips X'Pert-Pro X-ray diffractometer equipped with a back monochromator operating at 40 kV and a copper cathode as the X-ray source ($\lambda = 1.54$ Å).

DTA/TG

A simultaneous DTA/TG system (Perkin-Elmer Diamond DTA/TG) was used to analyze the thermal characteristics of the pure PVC, the sepiolite, and their nanocomposites from 20 to 1200°C at a heating rate of 10°C/min under a nitrogen atmosphere. The thermal degradation onset temperature and the thermal degradation weight loss of samples were also measured.

TEM and SEM

The samples were also investigated by TEM (FEI Tecnai G2 F30). The acceleration voltage was 200 kV. A scanning electron microscopy (FEI Quanta 200F) was used for clarifying the nanostructure composite. SEM samples were prepared on wafers

(chrome-coated pure silicon). Only one drop was dripped onto the wafer, and the solvent was allowed to evaporate. Working parameters are shown on SEM micrographs.

Surface Area of Samples

Surface areas (BET) of samples were measured using a Nova 2200e BET surface area instrument. The samples were loaded into a glass sample bulb and degassed at 150°C for 24 h. The surface area of the samples was obtained by using the BET method.

UV–Vis Spectra

The transmittance spectra of the nanocomposites in the range of 190–600 nm wavelengths were recorded by using a UV–vis spectrophotometer (Perkin Elmer Lamda 25).

FTIR–Attenuated Total Reflectance Spectra

Infrared spectra of samples were obtained by using a FTIR–attenuated total reflectance (ATR) (Perkin-Elmer Spectum One) spectrofotometer in the range of 4000–600 cm^{-1} in the transmission mode, and three scans were averaged.

Dynamic Mechanical Analysis

A dynamic-mechanical analyzer (Perkin Elmer Diamond DMA) was used to perform mechanical measurements from 25 to 120°C at 2 K min^{-1} on samples with different sepiolite amounts. The tests were carried out at a frequency of 1 Hz.

Results and Discussion

CHARACTERIZATION OF NANOCOMPOSITES

FTIR–ATR Analysis of Samples

FTIR–ATR Analysis of Sepiolite and Modified Sepiolite Samples. Figure 2 shows FTIR–ATR spectra of sepiolite and modified sepiolite samples in the zone of the spectrum between 4000 and 600 cm^{-1}. Natural sepiolite has a high content of different types of water (up to 16% of the total weight): physically adsorbed water, zeolitic water, and coordination or crystallization water. These different types of water differ on the strength of the link with the mineral. When sepiolite is heated, important changes are noticed not only in weight but also in morphology. Adsorbed and zeolitic water is eliminated at temperatures below 200°C. Coordinated water is lost at two stages: one half at the temperature range of 200–300°C and the other half at 350–550°C. The loss of coordination water involves structural changes resulting in a new phase, where the channel cross section is reduced and water loss is irreversible. The mineral with this new structure $[Si_{12}O_{30}Mg_8(OH)_4]$ is called anhydrous

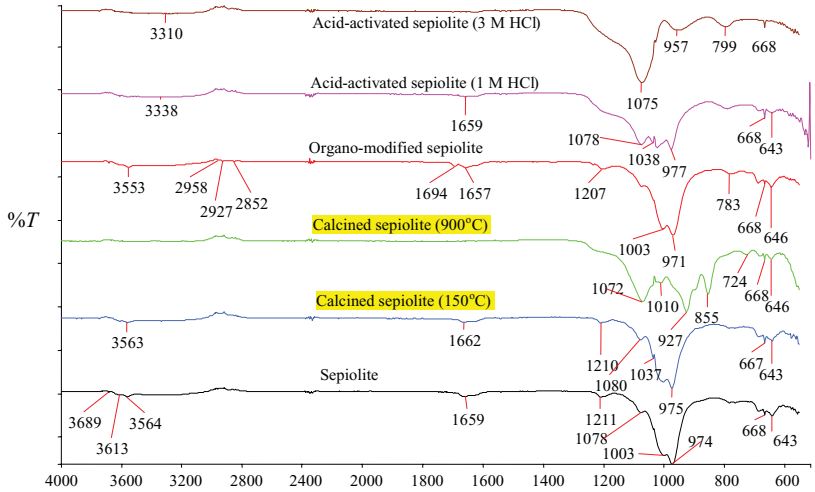

FIGURE 2. FTIR–ATR spectra of sepiolite and some modified sepiolite samples.

sepiolite. At this stage, the material has no water but it keeps silanol groups at the edge of the channels, and a temperature of 1100°C is necessary to destroy them.[29] FTIR–ATR spectra of the natural and calcined sepiolite samples are shown in Fig. 2. The Mg_3OH band at 3689–3564 cm^{-1} characterized by weak bonding strength is ascribed to the presence of OH groups in the octahedral sheet and the OH-stretching vibration in the external surface of the natural sepiolite. The —OH group in Mg_3OH corresponds to water bonded to magnesium ions in the octahedral layers. On the other hand, the 1659-cm^{-1} band is attributed to the OH stretching, representing the bound water coordinated to magnesium in the octahedral sheet. The Si—O coordination band at 1211 cm^{-1} represents the stretching of Si—O in the Si—O—Si groups of the tetrahedral sheet.[30] Increasing the calcination temperature produced a decrease in the bands corresponding to OH groups (643, 668, 1659, 3564, 3613, 3689 cm^{-1}) of water bonded to magnesium ions in the octahedral layer. On the other hand, the calcination treatment produces a decrease in the intensity of the Si—O band at 1211 cm^{-1}, which is typical for the tetrahedral layer of sepiolite. The higher temperature of calcination produces more noticeable changes in the FTIR–ATR spectra. Moreover, some peaks at higher temperatures disappeared. Therefore, the surface chemistry of the sepiolite was modified by the calcination procedure.

It is very easy to observe the organo modification of sepiolite with DMODCS due to a long-chain structure using FTIR–ATR spectra, as seen from Fig. 2. For example, the asymmetric and symmetric C—H stretching peaks resulting from alkyl groups at 2953, 2920, and 2851 cm^{-1} of DMODCS (not shown in Fig. 2) have shifted to 2958, 2927, and 2852 cm^{-1} due to the removal of a chlorine atom and being connected to the oxygen of Si. According to the explanation given above, the reaction between sepiolite and DMODCS may be written as the following:

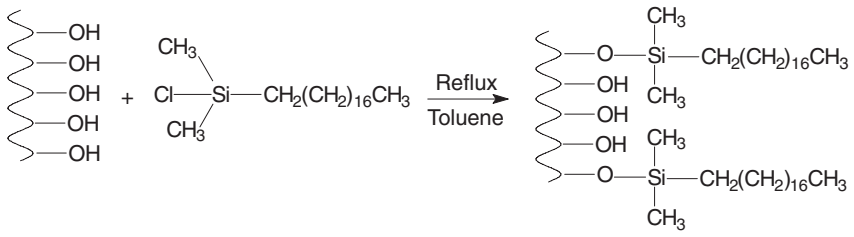

(1)

The spectra of natural sepiolite and acid-activated sepiolites (except for the activated sample with 0.5 M HCl) are shown in Fig. 2. As the treatment proceeds, the intensity of the bands due to the hydroxyl from the Mg_3OH group (3689 cm^{-1}) and to the different types of water existing in the natural sepiolite (3613 and 3564 cm^{-1}) decreased and finally disappeared. The band at 1659 cm^{-1}, due to the bending vibration mode of the water, underwent a similar simplification process. Likewise, the intensity of the bands situated between 1220 and 1000 cm^{-1}, characteristic of sepiolite and attributed to Si—O—Si vibrations, decreased and finally disappeared as the acid treatment progressed. As can be seen, there are some important changes in the intensity of some peaks after 24-h acid treatment at different acid concentrations. As the characteristic bands of the original silicate disappeared, new bands situated at 1220–1000 and 791 cm^{-1} appeared. These bands are characteristic of silica, although the shape of that at 1220–1000 cm^{-1} is different from that characteristic of the natural sepiolite.

FTIR–ATR Analysis of PVC and Its Nanocomposites. In the spectrum zone between 3200 and 2700 cm^{-1}, the absorption of energy is due to the stretching of C—H of different origins. The peaks in this zone for PVC and its nanocomposites may be due to C—H stretching of CHCl and CH_2. The zone between 2000 and 1150 cm^{-1} presents the bands of different origins such as those between 1800 and 1650 cm^{-1} due to the stretching of the C=O groups, those between 1650 and 1550 cm^{-1} corresponding to the C=C bonds, those at 1500–1400 cm^{-1} due to the wagging of the methylene groups, and those at 1330 and 1255 cm^{-1} due to the stretching of the C—H from ClCH groups.[31] As seen from Fig. 2, PVC and its nanocomposites have some peaks at these zones. The peak at 1426 cm^{-1} may be due to the wagging of the methylene groups and those at about 1332 and 1253 cm^{-1} are due to C—H deformations of CHCl. The last zone of the spectrum, between 700 and 600 cm^{-1}, corresponds to the stretching of the C—Cl bonds. From Fig. 3, PVC/calcined sepiolite nanocomposites

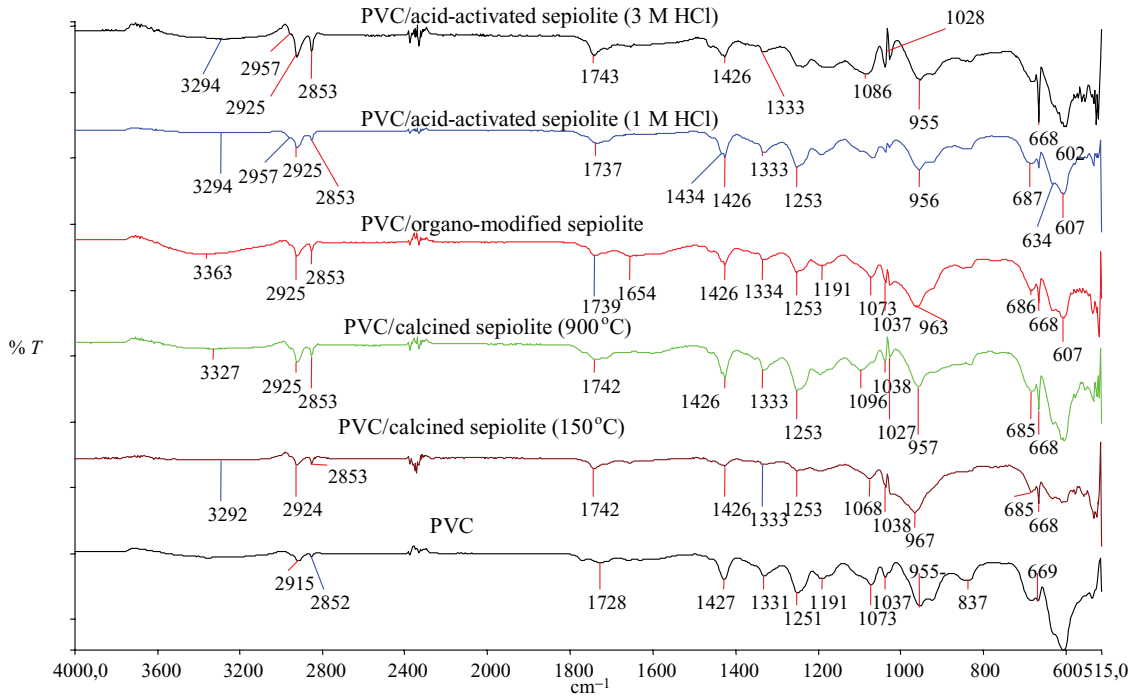

FIGURE 3. FTIR–ATR spectra of PVC and PVC/modified sepiolite nanocomposites.

exhibit the characteristic peaks of PVC, but as a result of calcination, some peaks of natural sepiolite have disappeared. It can be said that calcination brings into existence some differences in the structure of natural sepiolite. These differences may affect some properties of these types of nanocomposites. In the case of PVC/organo-modified sepiolite nanocomposites, there is a new peak at 3363 cm^{-1} due to the hydrogen bond formed between unmodified OH groups of natural sepiolite and the Cl atom of PVC. Moreover, the intensity of the peaks among 2953–2851 cm^{-1} of ≡CH and —CH_2 groups in the structure of PVC and modified sepiolite has increased due to overlapping of the peaks in this zone in the nanocomposite. Again, we have observed a shift at these peaks of the nanocomposite. A new peak at 3338 cm^{-1} on FTIR–ATR spectra of acid-activated sepiolite appeared, which may be due to the interactions between OH groups on the sepiolite surface and HCl (Fig. 3). In the nanocomposite case, there is a new peak at about 3294 cm^{-1} due to a hydrogen bond formed between —OH groups of unmodified sepiolite and Cl atoms of PVC. The other bands of pure PVC except for that at 1659 cm^{-1} due to the bending vibration mode of the water have almost appeared at the same point.

BET Surface Area Analysis of Sepiolite Samples

The surface areas of natural sepiolite and sepiolite samples calcined at 110, 150, 400, and 900°C were determined as 118, 307, 264, 161, and 90 m^2/g, respectively. As a result, surface area values decreased. Thus, the calcination modifies the surface chemistry and the crystalline structure of the sepiolite. The surface areas of natural sepiolite and sepiolite samples activated with 0.5, 1, and 3 M HCl solutions were 118, 460, 520, and 440 m^2/g, respectively. The results show that according to natural sepiolite, the surface area of sepiolites activated with 0.5 and 1 M HCl solutions increased and then decreased in the case of 3 M HCl solution. The effect of the acid treatment on the surface area can be ascribed to dissolution of the magnesium ions in the octahedral layer of sepiolite, which creates two new surfaces containing silanol groups, one facing the other.[32]

XRD Patterns of Samples

XRD Patterns of Sepiolite and Modified Sepiolites. XRD offers a convenient way to determine the interlayer spacing due to the periodic arrangement of the

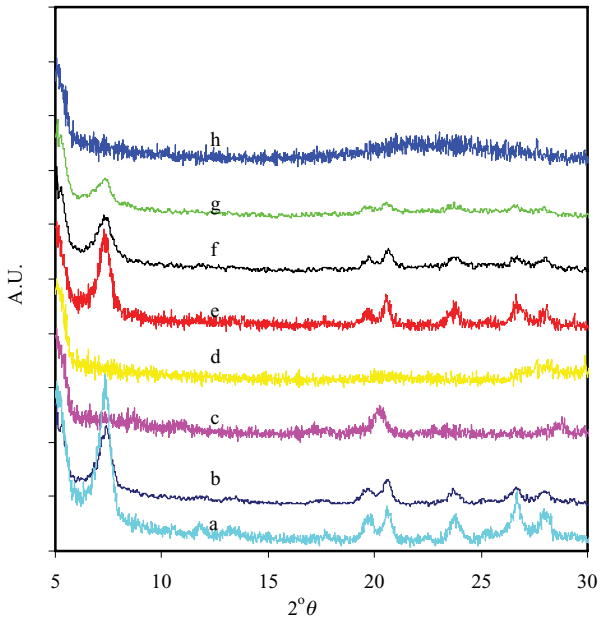

FIGURE 4. XRD patterns of (a) sepiolite, (b) calcined sepiolite (150°C), (c) calcined sepiolite (400°C), (d) calcined sepiolite (900°C), (e) organo-sepiolite, (f) activated sepiolite (0.5 MHCl), (g) activated sepiolite (1 M HCl), (h) activated sepiolite (3 M HCl).

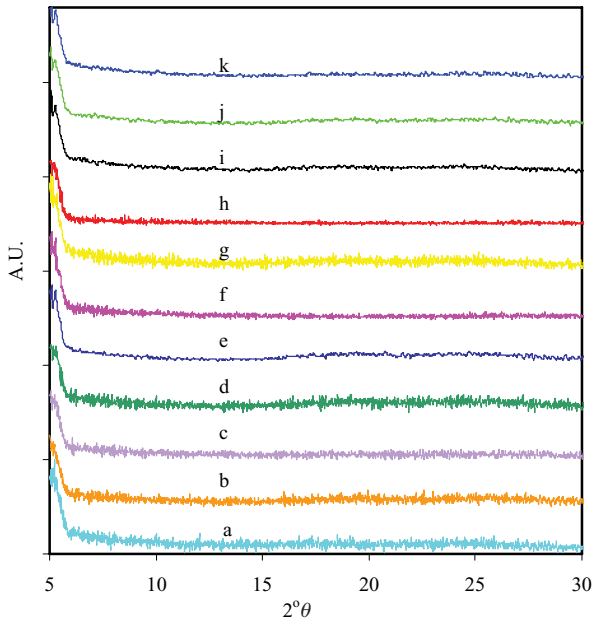

FIGURE 5. XRD patterns of (a) PVC, (b) PVC/sepiolite(1%), (c) PVC/sepiolite (2.5%), (d) PVC/sepiolite (5%), (e) PVC/calcined sepiolite (150°C, 2.5%), (f) PVC/calcined sepiolite (400°C) (2.5%), (g) PVC/calcined sepiolite (900°C, 2.5%), (h) PVC/organo-sepiolite (2.5%), (i) PVC/activated sepiolite (0.5 M HCl, 2.5%), (j) PVC/activated sepiolite (1 M HCl, 2.5%), (k) PVC/activated sepiolite (3 M HCl, 2.5%).

silicate layers in the clay and in intercalated polymer-layered silicate hybrids. Figure 4 shows the XRD patterns of sepiolite and modified sepiolites. Sepiolite has one sharp characteristic diffraction peak at $2\theta = 7.40°$. The XRD pattern of sepiolite, modified with DMODCS, shows that there is not any significant change in the XRD pattern of sepiolite with an organomodification process. But the calcination reduces the intensity of the line at $2\theta = 7.40°$. The calcination at 900° changes the XRD patterns, which forms the amorphous structure of sepiolite. From the XRD pattern of sepiolite samples treated with 0.5, 1, and 3 M HCl, it has been observed that the crystallinity of the samples decreased when the acid concentration was increased. Because the main peak of the sepiolite at $2\theta = 7.40°$ becomes less intense with the acid treatment.

XRD Patterns of PVC and Its Nanocomposites. Unlike montmorillonite layers, the sepiolite layers are linked by covalent bonds.[7] Figure 5 shows XRD patterns of PVC and PVC/modified sepiolite nanocomposites. It is known that PVC is an amorphous polymer. As shown in the figure, the disappearance of the basal peak at $2\theta = 7.40°$ for PVC/sepiolite nanocomposites is usually considered as evidence for good dispersion of sepiolite fibers. This change can be attributed to the fact that the texture in the sepiolite was altered in the sepiolite-filled nanocomposites, and then sepiolite was dispersed to fiber sticks or bundles and dispersed homogeneously into the PVC matrix. The intensity of the 110 peak is related to the volume fraction of sepiolite fibers, i.e., the lower the volume fraction of the fibers, the weaker the diffraction peak. In this study, similar results were also found for other PVC/modified sepiolite nanocomposites, as seen from Fig. 5. The basal peak of sepiolite for all these nanocomposites has not appeared due to the low volume fraction.

TEM Images of Sepiolite and PVC/Sepiolite Nanocomposite

We also carried out transmission electron microscopy to visualize the structure of the sepiolite. The TEM images can provide more direct evidence for the formation of nanocomposites. Also, TEM

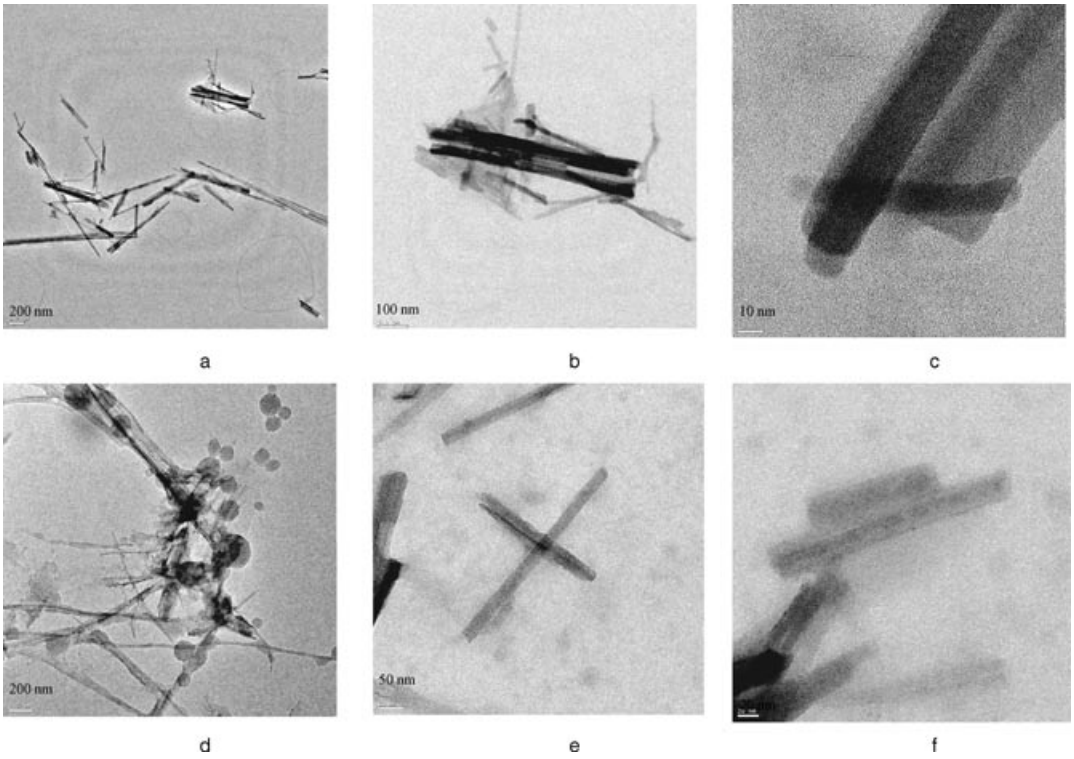

FIGURE 6. TEM images of sepiolite (a)–(c) and PVC/sepiolite nanocomposite (1 wt%) (d)–(f).

images support the fibrillar morphology of sepiolite. In this study, a TEM image of a PVC/sepiolite nanocomposite was obtained because the XRD pattern had not included the 110 peak of sepiolite at $2\theta = 7.40^{\circ}$, as mentioned before (Fig. 5). Figure 6 presents the TEM images of the sepiolite and PVC/sepiolite nanocomposite. In the TEM images of the sepiolite and PVC/sepiolite nanocomposite, the fiber bundles with the diameter, which are not uniform in nanoscale, are shown in Fig. 6. Sepiolite fibers have extremely long fiber structures. As seen from Figs. 6e and 6f, sepiolite needles are separated from each other in the PVC matrix. There is also some reduction in fiber length, as seen in Fig. 6f. The average diameter of sepiolite fibers is around 30 nm, and the length varies in the range of 100 to 700 nm. The average diameter of sepiolite fibers is around 30 nm, and the length varies in the range of 100 to 700 nm. Therefore, the aspect ratio is the range of 0.0428–0.3. Broken Si—O—Si bonds of the terminal silica tetrahedral are common phenomena for layered silicates and lead to the formation of silanol groups (Si—OH).[33] Different from montmorillonite (MMT), in which the presence of hydroxyl groups is only found on the edge of the aluminosilicate platelets, silanol groups are present on the whole external surface of sepiolite. The nanodispersion of sepiolite in the PVC matrix may be due to the interaction of the PVC chains with the Si—OH groups on sepiolite.[4] Figures 6d–6f show that most sepiolite fibers could be separately dispersed in the PVC matrix.

SEM Micrograph

Figure 7 shows the SEM micrograph of the sepiolite and PVC/sepiolite nanocomposite. The nanocomposite exhibits fibrous morphology, and a number of sepiolite fibers congregate into bundles. When Figs. 7a–7c and 7d–7f are compared with each other, the results demonstrate that the sepiolite bundles are broken down into the sepiolite fibers. The large aggregates of sepiolite fibers, as seen in Figs. 7a–c, are not observed in the PVC nanocomposites (Figs. 7d–7f). This confirms the good dispersion of sepiolite in the PVC matrix.

THERMAL PROPERTIES

To examine the thermal stability of sepiolite, thermal gravimetric and differential thermal analyses

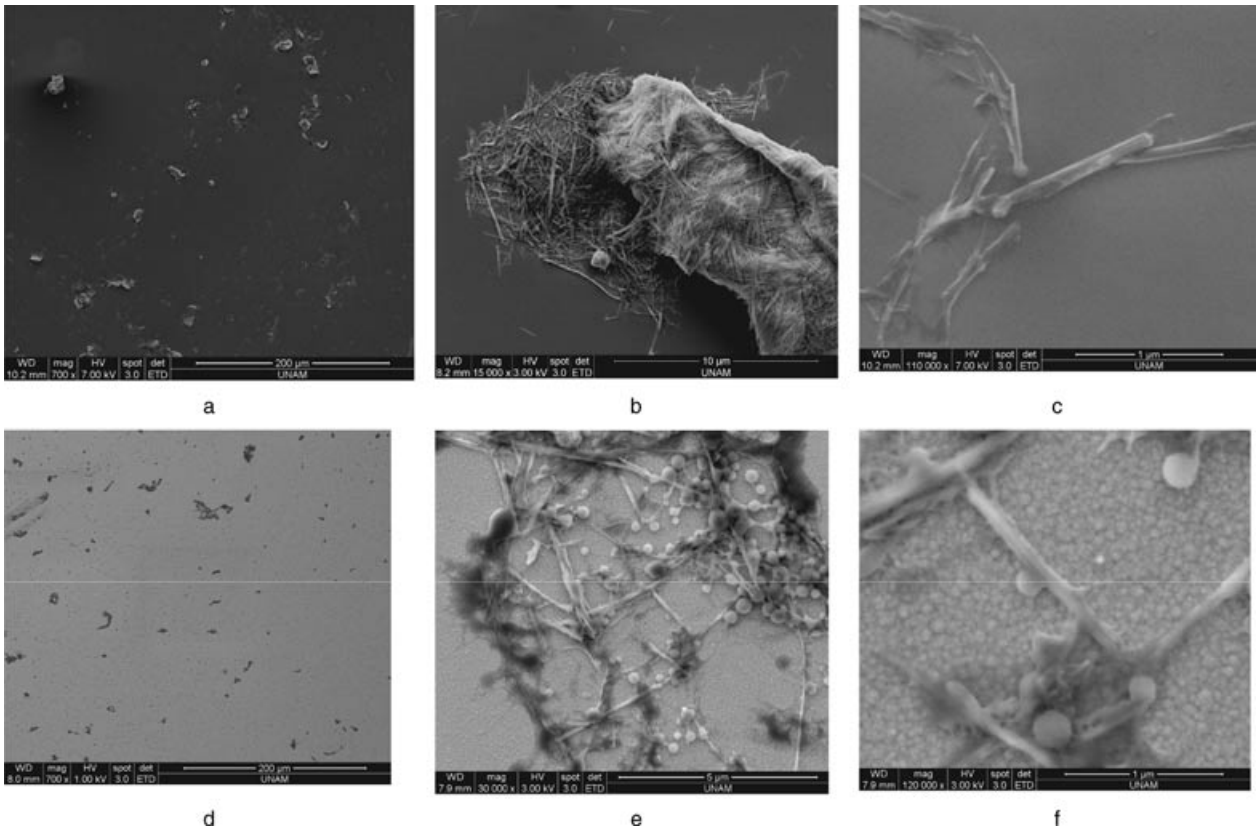

FIGURE 7. SEM images of sepiolite (a)–(c) and PVC/sepiolite nanocomposite (1 wt%) (d)–(f).

were carried out in the range of 20 and 1200°C in a static atmosphere of nitrogen. Figure 8 shows the TG, DTA, and d[TG] diagrams of sepiolite. In addition, to determine the calcination temperature of sepiolite, a TG study was carried out. The d[TG] curves were used to examine whether a change occurred in the thermal degradation mechanism of PVC. A total loss of mass in the range of 20 and 1200°C is shown in Fig. 8. The sepiolite samples show a loss of weight in the first region due to the removal of the physically adsorbed water molecules present. However, at a higher temperature, the losses have been assigned to the removal of chemisorbed water. The broad and strong exothermic peaks were noticed at 244, 336, and 843°C in the DTA curve, which can be assigned to the decomposition of sepiolite into an anhydrous compound.[34]

Many studies indicate that clay particles can improve the thermal stability of polymers, for instance, in cases where the polymer matrices are polystyrene,[11] poly(methyl methacrylate),[35,36] and polypropylene.[37] The presence of clay enhances the formation of char and hinders the diffusion of volatile decomposition products within the nanocomposites.[38] In practical applications, thermal properties are very important for PVC products. The temperatures and residue amount at weight losses 5, 10, 30, 50, and 80 phr, calculated from TG curves of PVC and its nanocomposites (figures not shown), are presented in Table I. As observed from the table, the temperatures and residue amount of nanocomposites prepared in various PVC/sepiolite ratios are higher than that of pure PVC over the tested temperature range, especially at a high temperature. These results reveal that the presence of sepiolite in the PVC matrix enhances the formation of the char, i.e., the carbonization of the polymer. These results indicate that PVC/sepiolite nanocomposites have better thermal properties than pure PVC at a high temperature. Similar results were also found by Liu et al. for PVC/layered double hydroxide nanocomposites,[39] Gong et al. and Peprnick et al. for PVC/montmorillonite nanocomposites,[38,40] and Yong-Zhong et al. for PVC/hydrotalcite

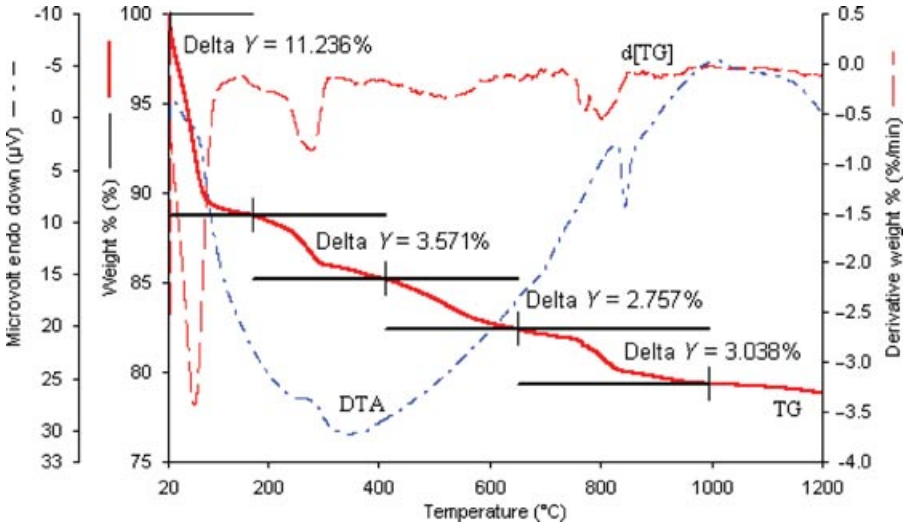

FIGURE 8. TG, DTA, and d[TG] diagrams of sepiolite.

nanocomposites.[41] Two weight loss stages with respect to the thermal degradation stages were observed in the TG curves. These stages are due to the thermal degradation of PVC. The first weight loss stage for PVC, occurring within the range of 280–300°C, is mainly due to the HCl elimination reaction of PVC molecules, followed by the formation of conjugated polyene sequences. The second weight loss stage, appearing within the range of 450–470°C, is due to the thermal degradation of the carbon chain of PVC, which produces flammable volatiles.[2,38]

Figure 9 shows the FTIR–ATR spectra of pure PVC and degraded PVC samples, which are heated for various periods such as 10, 30, 60, and 120 min at 300°C, which is the first degradation step temperature of PVC. PVC has characteristic FTIR–ATR peaks assigned to the C—Cl bond stretching vibrations in the range of 700–600 cm^{-1}, stretching C—H of CHCl at 2970 cm^{-1}, stretching C—H of CH_2 in 2912 cm^{-1}, deformation (Wagg) CH_2 in the range of 1435–1427 cm^{-1}, deformation C—H of CHCl at 1331–1255 cm^{-1}, stretching C—C in 1099 cm^{-1}, and rocking CH_2 at 966 cm^{-1}.[31] As seen from the FTIR–ATR spectrum in Fig. 9, the degradation of PVC at 300°C results in the formation of new peaks and a disappearance or decrease in the intensity of some peaks. For example, the intensity of the C—Cl bond stretching vibrations in the range of 700–600 cm^{-1} of pure PVC has disappeared with the degradation at 300°C. This shows that the release of HCl from the PVC backbone leads to the formation of double bonds. Again, the intensity of two bands corresponding to the C—H stretching of ClCH groups around 1330 and 1250 cm^{-1} decreases gradually and almost disappears as a consequence of the total elimination of chlorine atoms from the residue in the PVC. In Fig. 9, the peak of the C=C double bond at 1596 cm^{-1} is originated by dehydrochlorination from PVC during the thermal degradation step. Again, in the double bond zone in the range of 1650 and 1550 cm^{-1}, particularly in the range of 1590–1598 cm^{-1}, there are new peaks. This shows that the olefinic structure forms as a result of the elimination of HCl from PVC. According to the explanation given above, the degradation reaction of PVC can be written as

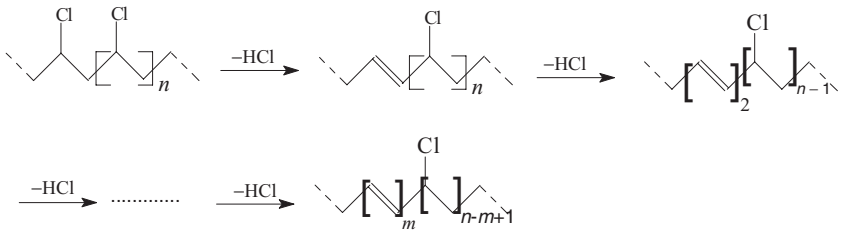

(2)

TABLE I
Thermal Stability Parameters of PVC and PVC/Sepiolite Nanocomposites

Samples	T_5 (°C)	T_{10} (°C)	T_{30} (°C)	T_{50} (°C)	T_{80} (°C)	Residue (%)
PVC Film	135	151	289	313	456	10.0
PVC/Sepiolite (1%)	143	159	290	315	460	11.5
PVC/Sepiolite (2.5%)	140	157	289	316	462	11.7
PVC/Sepiolite (5%)	139	161	292	318	485	16.8
PVC/activated sepiolite (0.5 M HCl) (2.5%)	137	173	297	322	476	13.9
PVC/activated sepiolite (1 M HCl) (2.5%)	128	166	295	320	473	13.6
PVC/activated sepiolite (3 M HCl) (2.5%)	150	189	280	305	470	11.0
PVC/calcined sepiolite (150°C) (2.5%)	131	172	296	320	472	12.5
PVC/calcined sepiolite (400°C) (2.5%)	157	219	282	307	479	13.5
PVC/calcined sepiolite (900°C) (2.5%)	163	247	292	316	479	13.7
PVC/organo-modified sepiolite (2.5%)	139	173	284	310	474	12.9

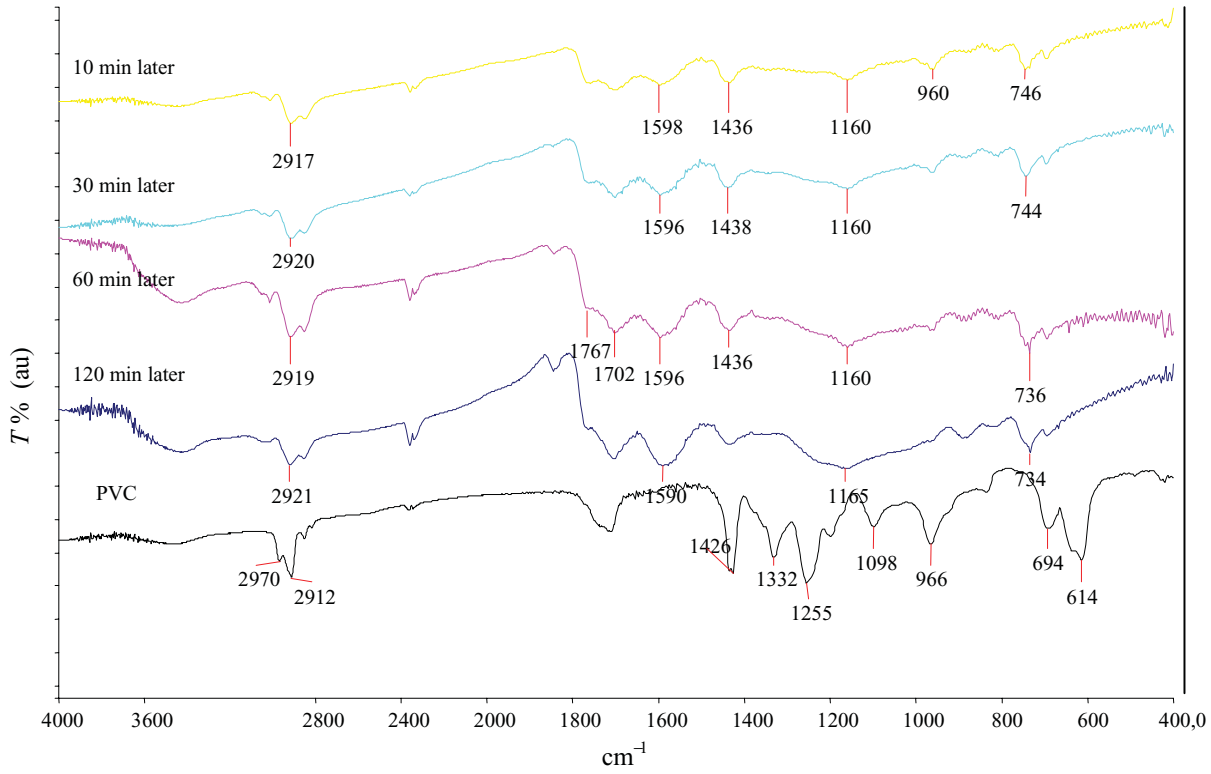

FIGURE 9. FTIR–ATR analysis for thermal degradation of PVC.

The degradation temperatures and residue amount presented in Table I for PVC/organo-modified sepiolite nanocomposites show that the thermal stability of nanocomposites was higher than that of PVC. The temperatures of the main degradation shift toward a higher value when organo-sepiolite is used, compared to the natural sepiolite. The thermal stability of PVC/calcined sepiolite nanocomposites increased depending on the increase in treatment temperature of sepiolite, as observed from Table I. The temperatures and residue amount have increased by sepiolite amount. Temperature and residue values reveal that the thermal stability strongly depends on PVC/clay interactions. Similar results were also found for PVC/acid-activated sepiolite nanocomposites, as observed from Table 1.

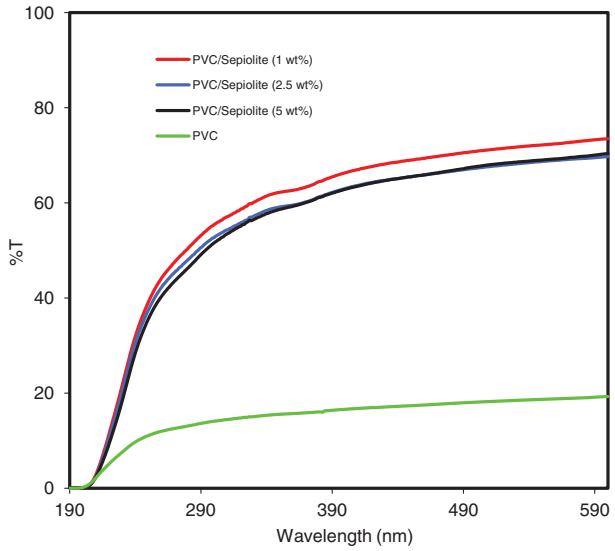

FIGURE 10. UV–vis transmittance spectra of PVC film and its nanocomposites.

OPTICAL BEHAVIOR

The optical properties of nanocomposite films are critical to their applications in some fields such as optical fiber coatings, lens coatings, and so forth. The weathering resistance of nanocomposite coatings also depends on their optical properties, especially their absorbance or transmission in the UV range.[42] Figure 10 shows the UV–vis transmission spectra of pure PVC film and PVC/sepiolite nanocomposites with 1, 2.5, and 5 wt% sepiolite. Because of the nanoscale dispersion of sepiolite layers in the PVC matrix, the transparency of the nanocomposites was better than that of PVC film due to improved intercalation. The spectra show that there were not any important changes in the transmission of nanocomposites with an increase in the sepiolite content and wavelength. In the range of 400–600 nm (visible light), more than 60% transmittance for all nanocomposites is observed. However, the transmittance of the nanocomposites has dramatically decreased in the range of 190–400 nm.

DYNAMIC MECHANICAL ANALYSIS

The storage modulus measures the stored energy, representing the elastic portion, and the loss modulus measures the energy dissipated as heat, representing the viscous portion.[43] Modulus values change with the temperature, and transitions in materials can be seen as changes in the E' or tan delta curves. This includes the glass transition temperature, and in this study, these values are calculated from the data presented in Fig. 11. The glass transition temperatures of PVC/sepiolite nanocomposites (1, 2.5, 5 wt%) are 72.3, 73.4, and 77.8°C, respectively. From the results, it is observed that the glass transition temperature increased with an increase in sepiolite loading. The effect of sepiolite loading on the mechanical properties of PVC nanocomposites is also shown in Fig. 11. With the incorporation of 1, 2.5, and 5 wt% sepiolite, the tensile strength is in the range of 26–39 MPa. The tensile strength of the PVC/sepiolite 2.5 wt% nanocomposite is higher than that of the other samples. This situation can explain a strong relationship between the morphology and mechanical behavior of the investigated PVC/sepiolite nanocomposites. A nanocomposite sample containing a smaller amount of clay can be better dispersed in a polymer matrix.

KINETIC ANALYSIS

Thermal stability is associated with both the initial temperature and the rate of degradation of polymers, so it is useful to determine the kinetic parameters by kinetic analysis for the degradation process. The reaction rate in TG studies can be defined as the variation of degree of conversion (α) with time or temperature, and the conversion is typically calculated as follows:

$$\alpha = \frac{W_0 - W_t}{W_0 - W_f} \tag{3}$$

where W_0, W_t, and W_f are, respectively, weight at the beginning of the degradation step, actual weight at each point of the curve, and the final weight measured after the specific degradation process considered.[44,45] TG curves for the first and second stages of PVC and the PVC/sepiolite nanocomposite under a nitrogen atmosphere at various heating rates (5, 10, 15, and 20°C/min) are shown in Figs. 12a and 12b. All curves are of approximately the same shape and indicate that the weight loss is independent of the heating rate. The degradation trend of the PVC/sepiolite nanocomposite is similar to that of pure PVC under a nitrogen environment. It is obvious that the PVC/sepiolite nanocomposite starts to degrade at a higher temperature than that of pure PVC. The total weight losses up to 600°C are 89.98%, 89.78%, 89.77%, and 90.19% at 5, 10, 15, and 20°C/min heating rates for pure PVC, and 84.22%, 85.01%, 84.32%, and 83.45% at 5, 10, 15,

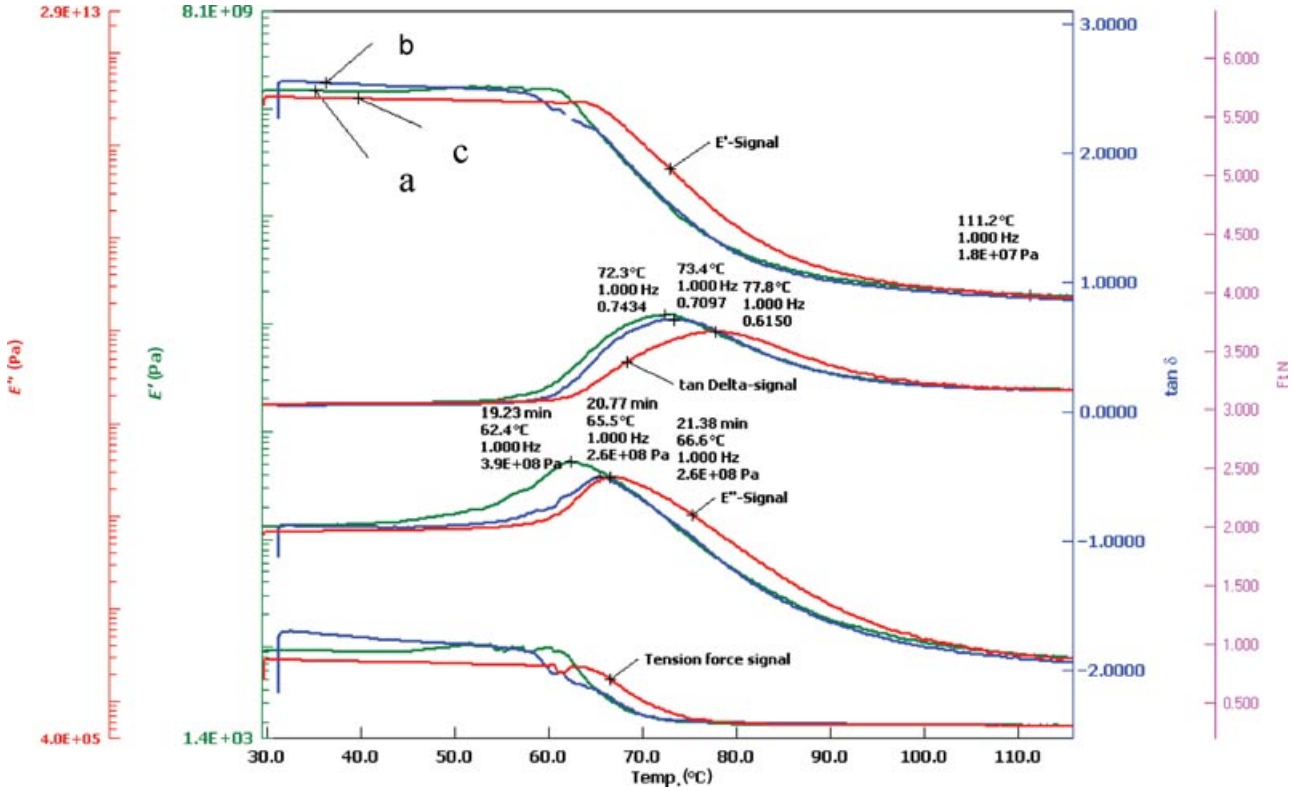

FIGURE 11. Dynamical mechanical analysis of nanocomposites: (a) PVC/sepiolite (1 wt%), (b) PVC/sepiolite (2.5 wt%), and (c) PVC/sepiolite (5 wt%).

and 20°C/min heating rates for the PVC/sepiolite nanocomposite, respectively. The onset degradation temperature T_{10} wt% at which the weight loss is 10%, the 50% weight loss temperature (T_{50} wt%), the first maximum weight loss temperature (T_{max1}), and the second maximum weight loss temperature (T_{max2}) of the PVC and PVC/sepiolite are summarized in Tables II and III, respectively. Both the T_{max1} and T_{max2} temperatures of the PVC and PVC/sepiolite nanocomposite shifted to high temperatures as the heating rate increased. The results obtained indicate that the presence of sepiolite may hinder the thermal degradation of PVC in the earlier degradation stage and thus may increase the thermal stability of the nanocomposites.

Since the Kissinger method was derived from the basic kinetic equations for heterogeneous chemical reactions and was not necessary to determine the reaction order or the conversional function, we used this method to calculate the kinetic parameters of pure PVC and the PVC/sepiolite nanocomposite. The utility of this method is that even without a precise knowledge of the reaction mechanism and reaction order, the activation energy can be

TABLE II
TG Data of PVC Obtained under a Nitrogen Atmosphere at Different Heating Rates

Heating Rate (°C/min)	$T_{10\%}$ (°C)	$T_{50\%}$ (°C)	T_{max1} (°C)	T_{max2} (°C)	Residue (%)
5	153	303	283	434	10.0
10	167	318	300	451	10.2
15	169	320	300	458	10.2
20	174	327	311	456	9.8

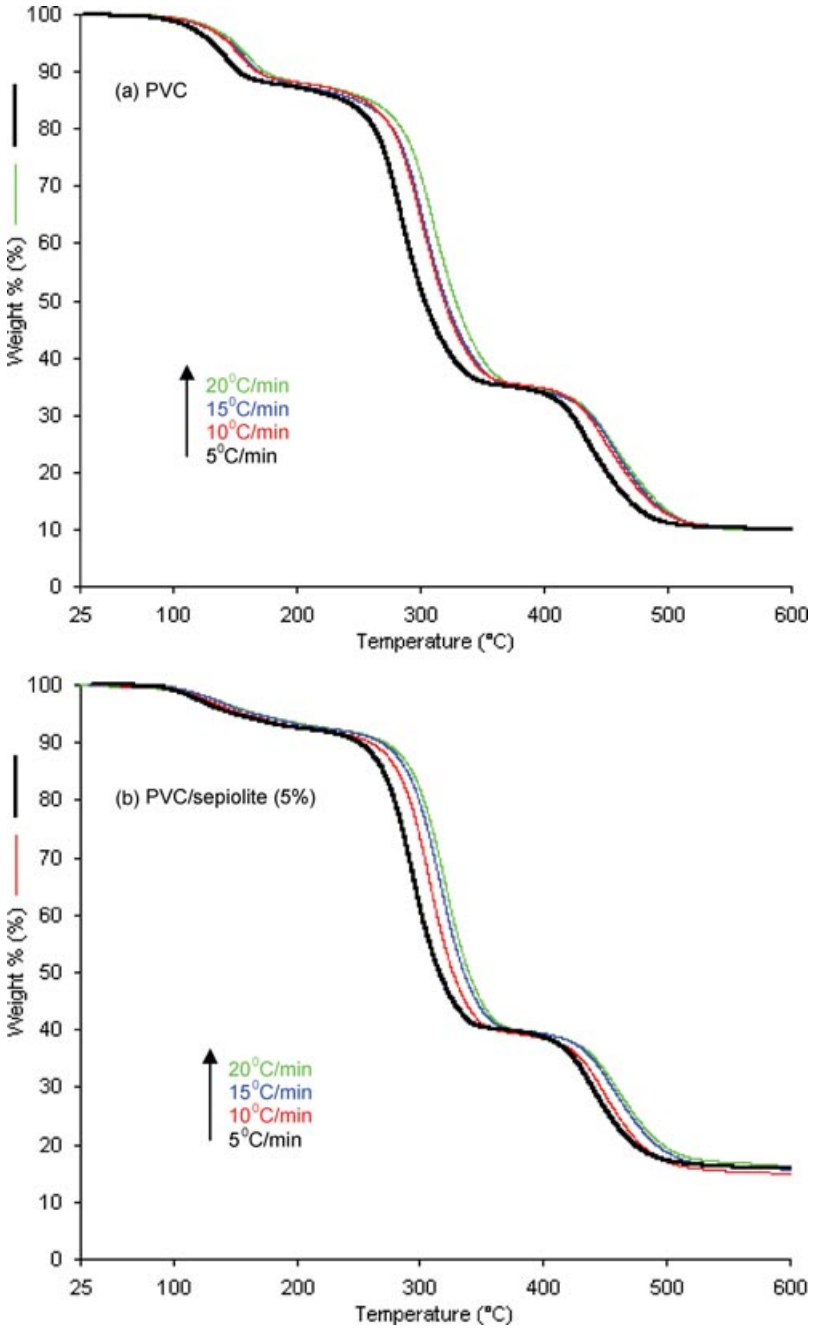

FIGURE 12. TG curves of (a) pure PVC and (b) PVC/sepiolite nanocomposite under a nitrogen atmosphere at four heating rates (5, 10, 15, and 20°C/min).

determined by using the following equation:

$$\ln\left(\frac{\beta}{T_{\max}^2}\right) = -\frac{E_a}{RT_{\max}} + \left\{\ln\frac{AR}{E_a} + \ln\left[n(1-\alpha_{\max})^{n-1}\right]\right\} \quad (4)$$

where β is the heating rate (°C/min), $T_{\max}$ is the temperature corresponding to the inflection point of the thermal degradation curves, which corresponds to the maximum rate (K), A is the preexponential factor, E_a is the activation energy, $\alpha_{\max}$ is the degree of conversion at the maximum rate, and n is the order of the reaction. From the slope of the

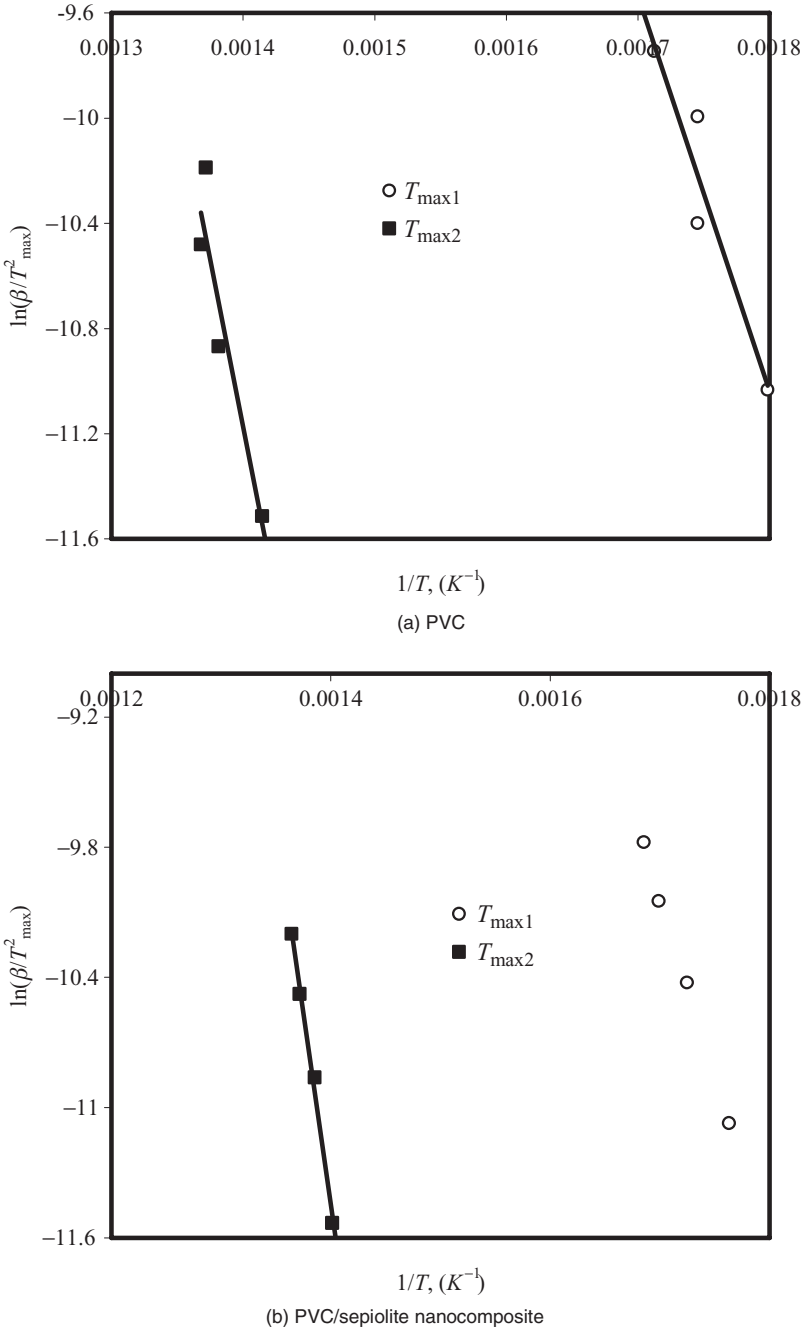

FIGURE 13. Plots used for the determination of the activation energies of (a) pure PVC and (b) its nanocomposite, consisting of 5 wt% sepiolite according to the Kissinger method.

plot of $\ln\left(\beta/T^2_{max}\right)$ versus $1/T_{max}$, E_a can be calculated. The Kissinger plots of the first and second degradation stages of PVC and its nanocomposite are shown in Figs. 13a and 13b. According to Eq. (4), E_a values were obtained by a linear regression using the least-squares method. The slopes change depending on the degree of conversion for the dehydrochlorination and decomposition reactions of PVC or the PVC/sepiolite nanocomposite. The activation energies of PVC and the PVC/sepiolite (5 wt%) nanocomposite are presented in Table IV. The results show that activation energy values at both stages for the PVC/sepiolite nanocomposite are higher than those of pure PVC, indicating that the

TABLE III
TG Data of PVC/Sepiolite Nanocomposite Obtained under a Nitrogen Atmosphere at Different Heating Rates

Heating Rate (°C/min)	$T_{10\%}$ (°C)	$T_{50\%}$ (°C)	T_{max1} (°C)	T_{max2} (°C)	Residue (%)
5	250	316	294	441	15.8
10	260	326	307	449	15.0
15	268	335	316	456	15.7
20	271	338	320	460	16.6

TABLE IV
Activation Energies of PVC and PVC/Sepiolite Nanocomposite (5%) by Using the Kissinger Method

Samples at Different Stages	Slope	E_a (kJ/mol)	R^2
PVC at the first stage of degradation	− 15,040	125	0.911
PVC at the second stage of degradation	− 25,439	211	0.882
PVC/sepiolite at the first stage of degradation	− 16,412	136	0.998
PVC/sepiolite at the second stage of degradation	− 35,238	292	0.992

addition of sepiolite particles improves the thermal stability of PVC. Similar results were found by Wan et al. for PVC/montmorillonite composites[46] and Dong et al. for polycarbonate/hydroxyapatite nanocomposites.[47]

Conclusions

PVC nanocomposites filled with sepiolite samples were prepared via the solution intercalation method. The TEM study demonstrated that the sepiolite particles were dispersed well in the PVC matrix. The experimental results revealed that organo modification, acid-activation, and calcination processes are effective methods to improve the thermal stability of PVC/sepiolite nanocomposites. Sepiolite enhances the formation of residue and improves the thermal stability of the polymer matrix. The thermal degradation kinetics of the PVC/sepiolite nanocomposite was studied by using the nonisothermal Kissinger method. The activation energy values calculated for two steps showed that the thermal stability of nanocomposites increased.

References

1. Wang, Q.; Zhang, X.; Dong, W.; Gui, H.; Gao, J.; Lai J.; Liu, Y.; Huang, F.; Song, Z.; Qiao, J Mater Lett 2007, 61, 1174.
2. Chen, G.; Tian, M.; Guo, S. J Macromol Sci Part B: Phys 2006, 45, 709.
3. Lee, LJ.; Zeng, C.; Cao, X.; Han, X.; Shen, J.; Xu, G. Composit Sci Technol 2005, 65, 2344.
4. Xie, X. L.; Li, R. K. Y.; Liu, Q. X.; Mai, Y. W. Polymer 2004, 45, 2793.
5. Wu, D.; Wang, X.; Song, Y.; Jin, R. J Appl Polym Sci 2004, 92, 2714.
6. Zeng, Q. H.; Yu, A. B.; Lu, G. Q.; Paul, D. R. J Nanosci Nanotechnol 2005, 5, 1574.
7. Chen, H.; Zheng, M.; Sun, H.; Jia, Q. Mater Sci Eng A 2007, 445–446, 725.
8. Liu, L. M.; Qi, Z. N.; Zhu, X. G. J Appl Polym Sci 1999, 71, 1133.
9. Guo, S.; Wu, H.; Chen, G.; Chen, X. Polym Compos 2003, 24, 456.
10. Pi, H; Guo, S.; Ning, Y. J Appl Polym Sci 2003, 89, 753.
11. Chen, G.; Guo, S.; Li, H. J. J Appl Polym Sci 2002, 86, 23.
12. Sun, S.; Li, C.; Zhang, l.; Du, H. I.; Burnell-Gray, J. S. Eur Polym J 2006, 42, 1643.
13. Demirbas, Ö.; Alkan, M.; Dogan, M.; Turhan, Y.; Namli, H.; Turan, P. J Hazardous Mater 2007, 149, 650.
14. Bradley, W. F. Am Mineral 1940, 25, 405.
15. Martin Vivaldi, J. L., Cano Ruiz, J. Anal Edaf (Madrid), 1953, 12, 827.
16. Nagy, B.; Bradley, W. F. Am Mineral 1955, 40, 885.
17. Jones, B. F.; Galan, E. Rev Mineral Geochem 1988, 19, 631.
18. Galan, E.; Carretero, M. I. Clays Clay Mineral 1999, 47, 399.
19. Dogan, M.; Türkyilmaz, A.; Alkan, M.; Demirbaş, Ö. Desalination 2009, 238, 257.
20. Yebra-Rodriguez, A.; Martin-Ramos, J. D.; Rey, F. D.; Viseras, C.; Lopez-Galindo, A. Clay Mineral 2003, 38, 353.
21. Turhan, Y.; Turan, P., Dogan, M.; Alkan, M.; Namli, H.; Demirbas, Ö. Indus Eng Chem Res 2008, 47, 1883.

22. Benlikaya, R.; Alkan, M.; Kaya, İ. Polym Compos 2009, 30, 1585.
23. Xie, S.; Zhang, S.; Wang, F.; Yang, M.; Seguela, R.; Lefebvre, J. M. Compos Sci Technol 2007, 67, 2334.
24. Ma, J.; Bilotti, E.; Peijs, T.; Darr, J. A. Eur Polym J 2007, 43, 4931.
25. Aranda, P.; Kun, R.; Martín-Luengo, M. A.; Letaïef, S.; Dékány, I.; Ruiz-Hitzky, E. Chem Mater 2008, 20, 84.
26. Santiago, F.; Mucientes, A. E.; Osorio, M.; Poblete, F. J. Polym Int 2006, 55, 843.
27. Darder, M.; Lpez-Blanco, M.; Aranda, P.; Aznar, A. A.; Bravo, J.; Ruiz-Hitzky, E. Chem Mater 2006, 18(6), 1602.
28. Doğan, M.; Alkan, M.; Onganer, Y. Water Air Soil Pollut 2000, 120, 229.
29. Gonzalez, L.; Rodrigez, A.; Marcos-Fernandez, A.; Del Campo, A. J Appl Polym Sci 2001, 79, 714.
30. Alkan, M.; Tekin, G.; Namli, H. Microporous Mesoporous Mater 2005, 84(1–3), 75.
31. Beltran, M.; Marcilla, M. Eur Polym J 1997, 33(7), 1135.
32. Aramendia, M. A.; Borau, V.; Corredor, J. I.; Jimenez, C.; Marinas, J. M.; Ruiz, J. R.; Urbano, F. J. J Colloid Interface Sci 2000, 227, 469.
33. Akyüz, S.; Akyüz, T. J Mol Struct 2003, 205, 651.
34. Darvishi, Z.; Morsali A. Appl Surf Sci 2010, 256, 3607–3611.
35. Blumstein, A. J Polym Sci Part A: Gen Pap 1965, 3, 2665.
36. Zhu, J.; Start, P.; Mauritz, K. A.; Wilkie, C. A. Polym Degrad Stab 2002, 77, 253.
37. Zanetti, M.; Camino, G.; Peichert, P.; Mulhaupt, R. Macromol Rapid Commun 2001, 22, 176.
38. Gong, F.; Feng, M.; Zhao, C.; Zhang, S.; Yang, M. Polym Degrad Stab 2004, 84, 289.
39. Liu, J.; Chen, G.; Yang, J. Polymer 2008, 49, 3923.
40. Peprnick, T.; Duchet, J.; Kovarova, L.; Malac, J.; Gerard, J. F.; Simonik, J. Polym Degrad Stab 2006, 91, 1855.
41. Yong-Zhong, B.; Zhi-Ming, H.; Shen-Xing, L.; Zhi-Xue, W. Polym Degrad Stab 2008, 93, 448.
42. Li, F.; Zhou, S.; Wu, L. J Appl Polym Sci 2005, 98, 1119.
43. Meyers, M. A.; Chawla K. K. Mechanical Behavior of Materials; Englewood Cliffs, NJ: Prentice-Hall, 1999.
44. Sengupta, R.; Sabharwal, S.; Bhowmick, A. K.; Chaki, T. K. Polym Degrad Stab 2006, 91, 1311.
45. Vyazovkin, S. Int Rev Phys Chem 2000, 9, 45.
46. Wan, C.; Tian, G.; Cui, N.; Zhang, Y.; Zhang, Y. J Appl Polym Sci 2004, 92, 1521.
47. Dong, Q. X.; Chen, Q. J.; Yang, W.; Zheng, Y. L.; Liu, X.; Li, Y. L.; Yang, M. B. J Appl Polym Sci 2008, 109, 659.